https://doi.org/10.33271/nvngu/2025-1/034

Y. Frolov,
orcid.org/0000-0001-6910-6223,
D. Konovodov*,
orcid.org/0000-0001-8282-4991,
O. Bobukh,
orcid.org/0000-0001-7254-3854,
V. Boiarkin,
orcid.org/0009-0005-7582-9504

Ukrainian State University of Science and Technology, Dnipro, Ukraine
* Corresponding author e-mail: d.v.konovodov@ust.edu.ua

TRANSFORMATION OF THE KIRIGAMI-TYPE DEFORMABLE INLAY DURING ROLL BONDING

Purpose. To quantitatively analyze the deformation of kirigami-type deformable inlays during the roll bonding process using soft outer matrices, with the goal of predicting their behavior within the composite structure.

Methodology. The research involved the fabrication of three-layer composite sheets through roll bonding. Expanded meshes made of mild steel and stainless steel served as the inlay phase, while copper and aluminum alloy sheets were employed as matrix materials. The transformation of the inlay phase within the composite sheets was evaluated.

Findings. The experimental investigation yielded data on the deformation behavior of kirigami-type inlays embedded within three-layer sheets during roll bonding. It was observed that using an aluminum matrix induces greater axial metal flow in the deformation zone, leading to a significant increase in the mesh distortion angle. A copper matrix primarily causes flattening of the mesh cells with minimal changes to their angular deformation. In contrast, rolling the steel mesh without a matrix results in negligible angular distortion until the rolling reduction exceeds 50 %.

Originality. This study represents the first quantitative analysis of the geometric transformation of kirigami-type deformable inlays as a function of deformation magnitude and matrix material properties during roll bonding. Understanding the shape transformation of the reinforcing phase within the composite sheet enables more accurate prediction of the contact area between the matrix materials during the bonding process.

Practical value. The findings of this research provide a basis for predicting the final geometry of kirigami structures within composite materials.

Keywords: *roll bonding, expanded steel mesh, aluminum matrix, copper matrix*

Introduction. Metal sheets and strips produced through rolling processes are extensively utilized in machine building. The ongoing trend toward reducing the weight of machinery and mechanisms, while maintaining necessary strength parameters, underscores the demand for sheet materials with enhanced mechanical properties. One promising approach to achieving such properties is the production of multilayer composites through roll bonding. Research efforts are actively focused on optimizing combinations of layers from diverse materials, including the application of reinforcing inlays of various shapes.

The deformation behavior of these reinforcing inlays during the rolling process presents a critical area of investigation. Understanding the extent of deformation of such inlays within a multilayer assembly is essential for predicting the strength and integrity of interlayer joining within the composite material.

Kirigami, a traditional Japanese art form that combines cutting and folding techniques to create intricate designs, has found innovative applications in engineering. This approach has been used to develop advanced structures and materials with unique mechanical, morphological, and functional properties. By incorporating controlled cuts and deformations, kirigami enables precise manipulation of material behavior, resulting in tunable mechanical properties and optimized interactions with various waves and fields.

Literature review. Expanded mesh is a particular case of the kirigami structure, which has a great potential in technic. Applying such structures to design of layered composite materials, which can be manufactured with roll bonding might eliminate the risk of excessive deformation and fracture of one of the layers. In this case, kirigami shape, for example, expanded steel mesh, used as a component of layered composite provides controlled discontinuities of deformation [1] during subsequent roll bonding. The thin sheet can be divided into two zones by the cutting scheme: a high strain zone and a low strain zone. The kinematic properties of the resultant structure can be programmed by the selection of a cutting pattern [2]. In this way, the kirigami technique opens the way to a programmable change in shape under the influence of a given load [3, 4], the acquisition of new mechanical properties, up to auxetic behavior [5]. Nowadays, the most popular effect, achieved via using of kirigami technic, is super-elasticity. It refers to the ability to extended elastic deformation with returning to initial shape after removing the load. Usually, super-elasticity is provided by elastomeric components. Most metallic materials cannot be stretched significantly, despite the clear advantages of doing so. For example, traditional batteries are stiff, however, adding of elasticity to them could provide new capabilities in soft robotics

[6] and wearable electronics devices [7]. Application of kirigami technique to multiplying the shape memory effect of Ni-Ti alloy was reported in [8]. Yang with co-authors recently reported [9] about a new class of electro-mechanical metamaterials inspired by transformable kirigami patterns has been developed for multiple electromagnetic applications. Kirigami inspired structures offers a scalable and easy-to-fabricate approach to impart elasticity beyond the constituent metallic materials. There have been many successful implementations on very stiff constitutive materials like graphene [10], SiN composite films [11], metallic glass [12] and similar. As a result, kirigami inspired components have shown broad application appeals, such as energy storage structures [13] shape-morphing systems, [14] flexible electronics, [15] sunlight tracking [16], robotic actuators [17] optics [18], stretchable heaters [19], and others.

If the classical kirigami approach means that the sheet from which the pattern is made is in most cases of negligible thickness, the rolling process works with the actual thickness of this sheet. Kirigami structures exhibit new properties after deformation by using precise cutting techniques of initial sheet materials. Namely, the deformation of the cut pattern defines the properties of the future structure and the entire composite when the kirigami structure is used as a structural element in it. A widely known representative of this type of structure is the expanded mesh with a rhombus cell shape.

Despite the effectiveness of using reinforcing phases to create composite materials, there is currently no reliable method for predicting the behavior of a rigid reinforcing phase in the middle of a soft matrix. The deformation of netting inlays for two different types of meshes during roll bonding in a low-oxygen environment [20] and hot rolling [21] was studied. The effect of the predictable transformation of the kirigami structure during the rolling process has been applied to the patterning of soft aluminum and copper matrices [20]. Such an effect has also been used in roll bonding of expanded-mesh composites, which is a particular case for kirigamized sheets of AISI 304 stainless steel [1] and AISI 1010 mild steel [22]. Various approaches have been taken to the shapes [23], sizes [24] of kirigami patterns in order to increase the tensile strength of the structure. In particular, it has been concluded that the tensile strength of kirigami structures produced by straight cross-cutting and curved cutting is similar, with a slight increase provided by curved cutting. Usage of effect of inhomogeneity of the stresses during the rolling on the mechanical properties of the finished product is widely known in umbilical stents and other bionic pipes, as well as at high precise cold rolled tubes. As demonstrated in reference [25], the mesh cell deforms in a relatively uniform manner until reaching a rolling reduction of 45 %. Beyond this threshold, the deformation of the mesh cells may become non-uniform. Fig. 1 shows the results of the authors' simulation of the axial tension (Fig. 1, *a*) and rolling (Fig. 2) of the kirigamized sheet with same initial patterns. The simulation was performed using the commercial FE software QForm UK [26] and clearly demonstrates the difference in the transformation of the kirigami structure depending on the type of deformation.

The findings of this study demonstrate that the rolling parameter can have a considerable impact on the 3D distribution of stress within the mesh elements and the deformation of the cells. It is therefore of the utmost importance to conduct a comprehensive investigation into the transformation of the inlay elements that have been deformed within the matrix during the rolling process.

Purpose. The aim of this study was to determine the transformation patterns of a kirigami-type deformable inlay during the roll bonding process using various matrix materials. Additionally, the research sought to provide a quantitative evaluation of the deformation characteristics of the individual elements within the mesh cells.

Methodology of experimental research. The reinforcing phase comprised an expanded mesh of two grades of steel, with the matrix consisting of sheets of aluminum and copper alloys.

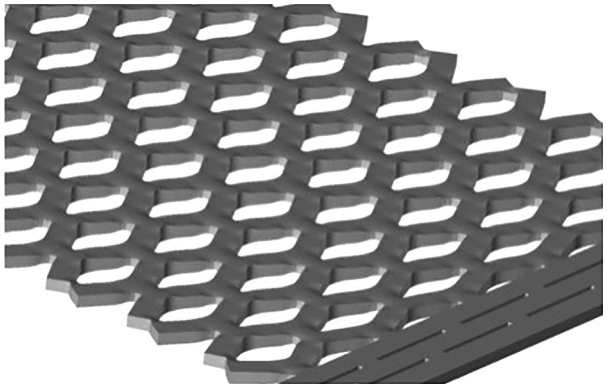

a

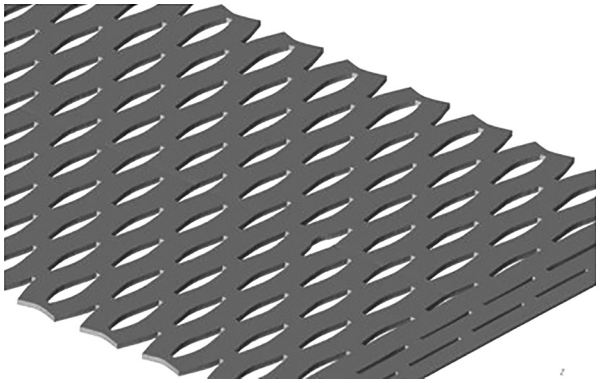

b

Fig. 1. Deformation of kirigamized sheet of steel DC01 with initial thickness 0.5 mm calculated using simulation software QForm UK:

a – tension; b – rolling

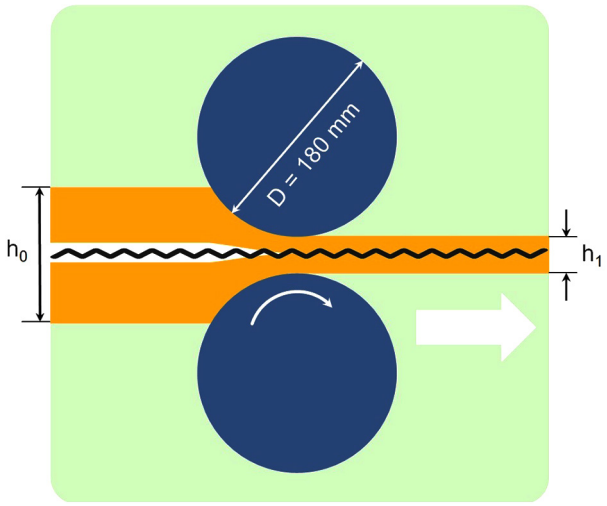

Fig. 2. The scheme of the roll bonding of the composite sheets

The first type of mesh is expanded steel mesh made from low carbon steel. It has the following characteristics according to the supplier's specification: material – steel DC/S235; type of mesh – TR-rhombic mesh; length of the cell – 6 mm; width of the cell – 3.7 mm; line – 0.5 mm; thickness of the sheet – 0.5 mm; format – 1,000 × 2,000 mm.

The following procedures, as reflected in their names, were used to prepare samples for further roll bonding:

$N_{St.}$ – cut for dimensions mesh was annealed at 720 °C within 10 minutes, freely cooled and carefully sand blasted.

$N_{St.}^{Cu}$ – the $N_{St.}$ sample additionally plated with Copper using galvanic procedure.

The second type of mesh is expanded steel mesh made from stainless steel: material (EN) – stainless steel 1.4301 (AISI 304); mesh form – diamond mesh; specification: 4 × 2.2 × 0.5 × 0.5; open area – 54 %; format of the sheet – 1,000 × 2,000 mm.

For preparation of samples of stainless expanded mesh, used the following procedures, which reflected in their name: N_{304} – cut for dimensions mesh was annealed at 1,050 °C within 5 minutes, rapidly cooled and carefully sand blasted.

The matrix joins the components of the further composite into a whole and provides the product with its shape. We used the followed materials as the matrix:

Al_1 – cut for dimensions aluminum sheet was annealed at 550 °C within 10 minutes, freely cooled and carefully sand blasted. Index in the name means the thickness of the sheet in mm.

Cu_1 – cut for dimensions copper sheet was annealed at 600 °C within 10 minutes, freely cooled and carefully sand blasted. Index in the name means the thickness of the sheet in mm.

The matrix material was cut to a size of 50 × 200 mm. The materials used were aluminium alloy AA1050 and copper alloy C10100. Their mechanical properties were determined by tensile testing, the results of which are presented in Table 1.

Prior to the roll bonding process, the mesh was positioned between two layers of the matrix material to form packages measuring 50 mm in width and 100 mm in length. Sheets of aluminum and copper alloy were folded in half, creating a cavity into which a steel mesh was inserted. No additional bonding agents or elements were employed to join the layers, thereby minimizing any potential influence on metal flow within the deformation zone. The overall rolling scheme for this composite configuration is illustrated in Fig. 2.

The packages were then rolled on two roll gap settings – 0.45 and 0.15 mm. The diameter of the working rolls was 180 mm. The rolling speed was equal to 15.6 m/min. The rolling process was carried out in two passes. In order to prevent the displacement of the matrix metal layers in relation to the steel mesh prior to their entry into the deformation zone, side guides were installed on the input side of the mill.

The expanded metal mesh was also rolled separately from the matrix material to get an idea of its deformability.

Results. In the course of development, some experiments were carried out to obtain data illustrating the influence of the matrix material on the deformation of the expanded mesh during cold roll bonding. The experimental schedule is as follows:

1. Rolling of the $N_{St.}$ and the N_{304} mesh samples without any matrix in three passes with roll gap 0.45 and 0.15 mm. (The initial thickness of both meshes is 0.5 mm).

2. Rolling of the $N_{St.}$ and the N_{304} mesh samples inside the aluminum as well as the copper matrix in two passes with rolling gap 0.45 an 0.15 mm (Initial thickness of the matrix-mesh assembly is 2.5 mm).

3. Measuring of the mesh geometry.

This allows one to get an idea of (Fig. 3) how the expanded mesh made of different steels deforms without any matrix (Columns *A* and *D* on the Fig. 3), as well as inside both: the relatively soft aluminum (Columns *B* and *E* in Fig. 3) matrix and the relatively hard copper (Columns *C* and *F* in Fig. 3) environment.

Table 1

The mechanical properties of aluminum and copper alloys

Alloy (UNS Number)	Tensile strength *Rm*, MPa	Yield strength $R_{p0.2}$, MPa	Shear modulus HPa
A91050	110	39	25.5
C10100	242	69	43.4
S30400	205	564	75.6
DC01*	232	330	82

* *according to EN 10130*

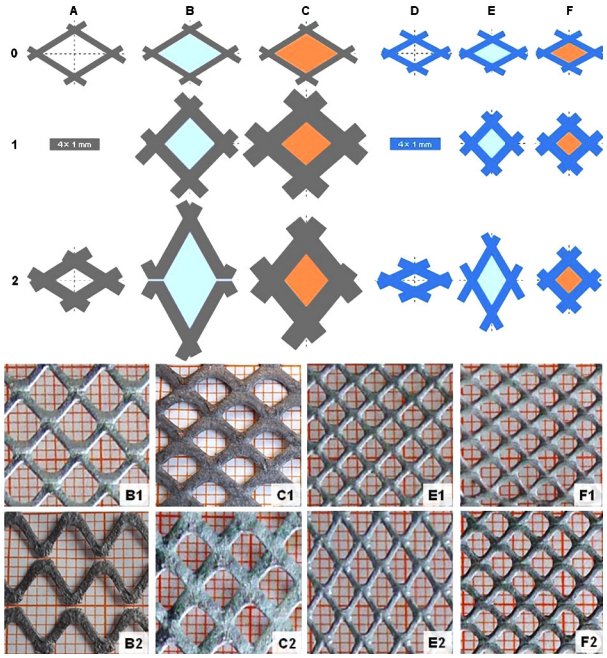

Fig. 3. Geometry of mesh cell after rolling in different environments:

a – visualization with saving of dimensional proportionality of the mesh cell; b – examples of deformed kirigami-type inlays. A0, B0, C0 – initial cell of the $N_{St.}$ with thickness h_0 of 0.5 mm; A2 – the cell of the $N_{St.}$ after rolling without any matrix to thickness h_2 = 0.33 mm; B1 – the cell of the $N_{St.}$ after rolling inside aluminum matrix to thickness h_1 = 0.49 mm; B2 – the cell of the $N_{St.}$ after rolling inside aluminum matrix to thickness h_2 = 0.41 mm. The breakage of the mesh observed; C1– the cell of the $N_{St.}$ after rolling inside copper matrix to thickness h_1 = 0.41 mm; C2 – the cell of the $N_{St.}$ after rolling inside copper matrix to thickness h_2 = = 0.33 mm; D0, E0, F0 – initial cell of the N_{304} with thickness h_0 of 0.5 mm; D2 – the cell of the N_{304} after rolling without any matrix to thickness h_2 = 0.38 mm E1 – the cell of the N_{304} after rolling inside aluminum matrix to thickness h_1 = 0.49 mm; E2 – the cell of the N_{304} after rolling inside aluminum matrix to thickness h_2 = = 0.45 mm; F1– the cell of the N_{304} after rolling inside copper matrix to thickness h_1 = 0.49 mm; F2– the cell of the $N_{St.}$ after rolling inside copper matrix to thickness h_2 = 0.33 mm

The results of the experiments were used to investigate the transformation of grids resulting from deformation. The transformation of the mesh cells was observed and documented using an optical microscope. Images of the expanded steel mesh, after deformation within the matrix material, are presented in Fig. 3.

An evaluation of the shapes of the inlays revealed significant differences in the change of cell shape during rolling in both aluminum and copper matrices. It is important to highlight the fact that this phenomenon is related to the difference in the ductile properties of the matrix materials in relation to the inlay. Although both inlays show similar responses when rolled within either the aluminum or copper matrix (*B*1~*E*1; *C*1~*F*1; *B*2~*E*2; *C*2~*F*2), the effect of the surrounding matrix material differs. Specifically, aluminum primarily causes thinning of the lines (*B*1; *B*2; *E*1; *E*2), while copper induces a predominant flattening of the inlay.

The characteristic dimensions of the mesh cell are presented in Fig. 4.

Measured values of the characteristic dimensions of the mesh cell presented from Fig. 4 are given in Table 2: L_1 – widening of the mesh line is general tendency for all experiments. This seems like the major deformation for rolling of general steel mesh in copper matrix. Nevertheless, the contraction of the width observed for stainless steel mesh in both environ-

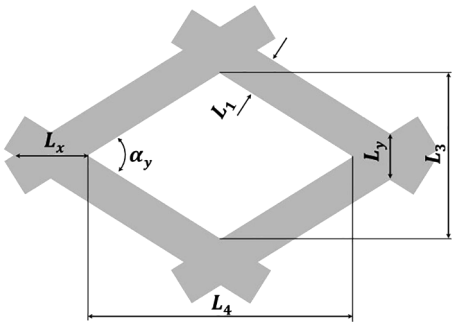

Fig. 4. Scheme of the cell dimensions

ments after the second pass. L_3 – the diagonal of the cell alongside the rolling direction demonstrates a different behavior depending on presence of the matrix: it contracts significantly without it, but growths with both types of matrixes. L_4 – the cross diagonal of the cell contracts in all experiments, excepting mesh in both environments after the second rolling pass. This exception could be explained by contracting of L_1 in conditions of low intensity of the growth of the angle α_y. L_y – increases in all performed experiments. L_x – demonstrates significant enlargement during the rolling without matrix as well as in first pass of rolling of general steel mesh in copper matrix. Its related to the flattering of the mesh line L_1.

The cell area A_c (Table 2) is an important characteristic of a composite material. It determines the geometric stiffness of the composite. It also determines the transparency of the composite to wave radiation. Under matrixless rolling conditions, the cell area is reduced by 63 and 54 % for general and stainless steel, respectively. This is due to the flattening of the mesh lines. At the same time, the rolling of general steel mesh in an aluminum matrix results in the most intensive growth of A_c in both after the first (7 %) and second (99 %) passes. For stainless steel, the growth reaches 10 and 72 %, respectively. When rolling is performed in a copper matrix, the first pass results in a significant reduction of the A_c (10 and 12 %) for general and stainless steel meshes, respectively. In the second pass, the mesh area begins to increase slightly.

In addition to the cell area itself, it is also useful to evaluate the anisotropy of the linear dimensions through the ratio of the L_3 and L_4 values – $D_{3/4}$ (Table 2). The anisotropy remains largely unchanged when the mesh is rolled without a matrix. However, the most significant impact on the anisotropy of the cell geometry occurs when the mesh, whether steel or stainless steel, is rolled within the aluminum matrix. In contrast, when using a copper matrix, significant elongation of the cell structure is notably more difficult to achieve.

Angle α_y. This angle is a clear marker of axial flow of the inlay inside the matrix.

Analysis of changing of the values from Table 1 performed using following tools.

Linear dimensions as well as the angle

$$\ln(h;L;\alpha) = \ln\left(\frac{(h;L;\alpha)_i}{(h;L;\alpha)_{i-1}}\right). \quad (1)$$

Cell area

$$dA_c = \left(\frac{A_{c(i-1)} - A_{c(i-1)}}{A_{c(i-1)}}\right)\cdot 100\ \%. \quad (2)$$

Ratio of the cells diagonals

$$dL_{3/4} = \left(\frac{L_{\frac{3}{4}(i-1)} - L_{\frac{3}{4}(i)}}{L_{\frac{3}{4}(i-1)}}\right)\cdot 100\ \%. \quad (3)$$

The change in the of the mesh geometry values, as calculated by formulas (1–3) with the data from Table 2 are illustrated in Table 3.

The main conclusion that clearly emerges from the data is as follows:

The cell area decreases (–64 and –54 %) during rolling without matrix, increases continuously during rolling in soft aluminum matrix (8 and 100 % for general steel mesh; 10 and 72 for stainless steel mesh), and shows alternating behavior during rolling in copper matrix. Thus, the cell area shrinks in the first pass and then grows in the second pass (–10 and +7 % for common steel mesh; –20 and +23 % for stainless steel mesh).

The width of the mesh line always increases when rolling it without a matrix. Nevertheless, it seems very unlikely that the cell is completely closed.

The factor, which helps quantitatively describe the degree

Table 2

Measured and calculated values of mesh according to Figs. 3 and 4

Exp. code	h_i in mm	L_1 in mm	L_3 in mm	L_4 in mm	L_y in mm	L_x in mm	α_y in deg.	A_c in mm^2	$D_{3/4}$
*A*0	0.50	0.50	3.12	5.00	0.58	1.00	64	0.62	0.58
*A*2	0.33	0.99	1.88	3.00	1.15	1.89	56	0.63	2.17
*B*0	0.50	0.50	3.12	5.00	0.58	1.00	64	0.62	0.58
*B*1	0.49	1.00	4.20	4.00	1.41	1.40	94	1.05	1.97
*B*2	0.41	1.01	7.80	4.30	2.05	1.15	122	1.81	2.36
*C*0	0.50	0.50	3.12	5.00	0.58	1.00	64	0.62	0.58
*C*1	0.41	1.40	3.50	4.00	1.84	2.14	82	0.88	3.94
*C*2	0.33	1.55	4.30	3.50	2.42	2.00	102	1.23	4.84
*D*0	0.50	0.50	1.62	3.00	0.58	1.00	58	0.54	0.58
*D*2	0.38	0.76	1.01	2.20	0.80	1.81	50	0.46	1.45
*E*0	0.50	0.50	1.62	3.00	0.58	1.00	58	0.54	0.58
*E*1	0.49	0.71	2.40	2.23	1.02	0.96	94	1.08	0.98
*E*2	0.45	0.68	4.00	2.30	1.31	0.77	122	1.74	1.01
*F*0	0.50	0.50	1.62	3.00	0.58	1.00	58	0.54	0.58
*F*1	0.49	0.80	1.88	2.07	1.05	1.17	84	0.91	1.23
*F*2	0.43	0.75	2.18	2.20	1.13	1.15	88	0.99	1.30

Table 3

Changing of values of mesh geometry according to Table 2 and formulas (1–3)

Exp. code	$\ln_{h_i}$	$\ln_{L_1}$	$\ln_{L_3}$	$\ln_{L_4}$	$\ln_{L_y}$	$\ln_{L_x}$	$\ln_{\alpha_y}$	dA_c in %	dL_3 in %
*A*2	–0.42	+0.68	–0.51	–0.51	+0.68	+0.64	–0.13	–64	+0
*B*1	–0.02	+0.69	+0.3	–0.22	+0.89	+0.34	+0.38	+8	+68
*B*2	–0.18	+0.01	+0.62	+0.07	+0.37	–0.2	+0.26	+100	+73
*C*1	–0.20	+1.03	+0.11	–0.22	+1.15	+0.76	+0.25	–10	+40
*C*2	–0.22	+0.10	+0.21	–0.13	+0.27	–0.07	+0.22	+7	+40
*D*2	–0.27	+0.42	–0.47	–0.31	+0.32	+0.59	–0.15	–54	–15
*E*1	–0.02	+0.35	+0.39	–0.3	+0.56	–0.04	+0.48	+10	+99
*E*2	–0.09	–0.04	+0.51	+0.03	+0.25	–0.22	+0.26	+72	+62
*F*1	–0.02	+0.47	+0.15	–0.37	+0.59	+0.16	+0.37	–20	+68
*F*2	–0.13	–0.06	+0.15	+0.06	+0.07	–0.02	+0.05	+23	+9

of the cell closure, is the ratio of cross diagonal of the cell L_4 to cross diagonal of the mesh knuckle L_x (Fig. 4).

It is important to emphasize that the reported thickness of the mesh after deformation should be interpreted as an average value, as the observed changes in mesh thickness were not uniform. These changes included not only the expected reduction in thickness but also instances of thickness increase. Computer simulations of mesh tension, performed using QForm software, reveal areas of significant compressive stress that arise from the "opening" of the mesh, particularly in the knuckles. This stress induces plastic deformation in localized regions, with the metal flow occurring perpendicular to the rolling direction. Consequently, the observed increase in mesh thickness corresponds to the well-known "barreling" effect seen on the side surfaces of the compressed specimen. This phenomenon accounts for the delayed reduction in mesh thickness relative to other deformation parameters, as it results from the measurement of the maximal value. Fig. 5 illustrates the visualization of the thickness increase effect during the tension of the cut sheet (*a*) and (*b*), and after the mesh is rolled within the aluminum matrix (*c*).

The simulation data presented in Fig. 5 indicate that thickness inhomogeneity is more pronounced during the tension process. In zone *2*, the thickness reaches 0.54 mm, whereas the initial thickness of the sheet was only 0.5 mm (Fig. 5, *b*). It is important to note that the inhomogeneity of the thickness, which originates during the rolling process, is also clearly observable, although it exhibits a more gradual variation compared to the tension phase. Thus, the variation of the thickness of the inlays is not homogeneous, due to the increase in the mesh angle α_y (angle of the mesh along the rolling direction). The angle 180° – α_y (angle of the mesh across the rolling direction) is closing, which induces deformation of compression near its apex.

The discussion of the obtained results could be based on the controlled inhomogeneity of the deformation inside the matrix. This inhomogeneity inspires the appearance of the complex 3D interface between the inlay and the matrix. The shape of this interface depends on the interaction of two materials during their plastic flow through the deformation zone during rolling. The measurable parameters of such interaction remain uncovered, that is, what the physical of artificial indicator that can predict the flow of the inlay: either as in the aluminum (columns *B* and *E* in Fig. 3) or as in the copper (columns *C* and *F* in Fig. 3) is not yet designed. The proper tool for solving of the such task – FE simulation and its features involved in the solution, which is called to open an avenue for increasing of mechanical properties of the composites. The complex 3D arcuate shape of the interface when modified with intermetallic phases could add geometric stiffness to the composite. Due to the programmable direction of mutual diffusion of composite components, this effect plays a crucial role in solid state alloying.

Conclusions. It has been established that:

1. The shape of the kirigami structure inside roll bonded composites is derived from dynamic equilibrium of mechanical as well as ductile properties of both inlay and matrix materials along deformation zone in complex heat conditions.

2. The "softer" is the matrix, the higher is the axial flow in the zone of deformation. This leads to a significant increase in the angle of the kirigami structure as well as thinning of its lines.

3. The "hard" matrix forces the kirigami structure to flatten instead of changing its angle, as in the copper experiments described above.

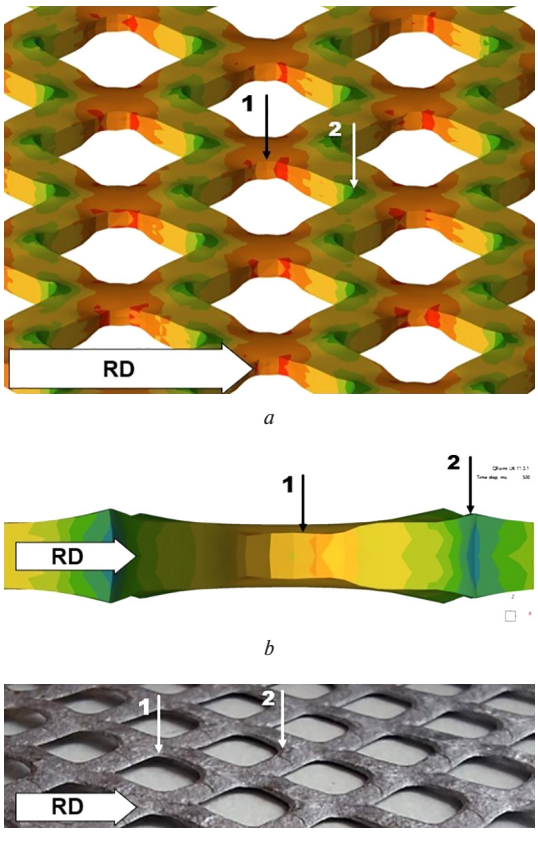

Fig. 5. Visualization of thickness inhomogeneity, induced during the tension of cut sheet (*a*) *– dimetric view and* (*b*) *– side view, and after rolling of the mesh inside aluminum matrix* (*c*):

1 – thin zone; 2 – thick zone

Acknowledgements. *The research was conducted during the implementation of project No 2023.04/0156 "Development of technology for the use of kirigami structures in the deformation-thermal processing of composite materials", which received a grant from the National Research Foundation of Ukraine within the competition "Science for strengthening the defense capability of Ukraine".*

References.

1. Frolov, Y., Haranich, Y., Bobukh, O., Remez, O., Voswinkel, D., & Grydin, O. (2020). Deformation of expanded steel mesh inlay inside aluminum matrix during the roll bonding. *Journal of Manufacturing Processes, 58*, 857-867. https://doi.org/10.1016/j.jmapro.2020.08.049.
2. Tao, J., Khosravi, H., Deshpande, V., & Li, S. (2022). Engineering by Cuts: How Kirigami Principle Enables Unique Mechanical Properties and Functionalities. *Advanced Science,* 2204733. https://doi.org/10.1002/advs.202204733.
3. Jin, L., Forte, A. E., Deng, B., Rafsanjani, A., & Bertoldi, K. (2020). Kirigami-Inspired Inflatables with Programmable Shapes. *Advanced Materials, 32*(33), 2001863. https://doi.org/10.1002/adma.202001863.
4. Hwang, D.-G., & Bartlett, M. D. (2018). Tunable Mechanical Metamaterials through Hybrid Kirigami Structures. *Scientific Reports, 8*(1). https://doi.org/10.1038/s41598-018-21479-7.
5. Neville, R. M., Scarpa, F., & Pirrera, A. (2016). Shape morphing Kirigami mechanical metamaterials. *Scientific Reports, 6*(1). https://doi.org/10.1038/srep31067.
6. Zhang, Y., Li, P., Quan, J., Li, L., Zhang, G., & Zhou, D. (2022). Progress, Challenges, and Prospects of Soft Robotics for Space Applications. *Advanced Intelligent Systems,* 2200071. https://doi.org/10.1002/aisy.202200071.
7. Song, W., Yoo, S., Song, G., Lee, S., Kong, M., Rim, J., Jeong, U., & Park, S. (2019). Recent Progress in Stretchable Batteries for Wearable Electronics. *Batteries & Supercaps, 2*(3), 181-199. https://doi.org/10.1002/batt.201800140.
8. Wang, W., Rodrigue, H., Kim, H.-I., Han, M.-W., & Ahn, S.-H. (2016). Soft composite hinge actuator and application to compliant robotic gripper. *Composites Part B: Engineering on Science Direct, 98,* 397-405. https://doi.org/10.1016/j.compositesb.2016.05.030.
9. Yang, Y., Vallecchi, A., Shamonina, E., Stevens, C. J., & You, Z. (2023). A new class of transformable kirigami metamaterials for reconfigurable electromagnetic systems. *Scientific Reports, 13*(1). https://doi.org/10.1038/s41598-022-27291-8.
10. Blees, M. K., Barnard, A. W., Rose, P. A., Roberts, S. P., McGill, K. L., Huang, P. Y., ..., & McEuen, P. L. (2015). Graphene kirigami. *Nature, 524*(7564), 204-207. https://doi.org/10.1038/nature14588.
11. Hashimoto, M., & Taguchi, Y. (2020). Design and Fabrication of a Kirigami-Inspired Electrothermal MEMS Scanner with Large Displacement. *Micromachines, 11*(4), 362. https://doi.org/10.3390/mi11040362.
12. Han, D. X., Zhao, L., Chen, S. H., Wang, G., & Chan, K. C. (2021). Critical transitions in the shape morphing of kirigami metallic glass. *Journal of Materials Science & Technology, 61,* 204-212. https://doi.org/10.1016/j.jmst.2020.05.065.
13. Gong, X., Yang, Q., Zhi, C., & Lee, P. S. (2020). Stretchable Energy Storage Devices: From Materials and Structural Design to Device Assembly. *Advanced Energy Materials,* 2003308. https://doi.org/10.1002/aenm.202003308.
14. Babaee, S., Pajovic, S., Rafsanjani, A., Shi, Y., Bertoldi, K., & Traverso, G. (2020). Bioinspired kirigami metasurfaces as assistive shoe grips. *Nature Biomedical Engineering, 4*(8), 778-786. https://doi.org/10.1038/s41551-020-0564-3.
15. Kim, K. K., Suh, Y., & Ko, S. H. (2020). Smart Stretchable Electronics for Advanced Human–Machine Interface. *Advanced Intelligent Systems,* 2000157. https://doi.org/10.1002/aisy.202000157.
16. Lamoureux, A., Lee, K., Shlian, M., Forrest, S. R., & Shtein, M. (2015). Dynamic kirigami structures for integrated solar tracking. *Nature Communications, 6*(1). https://doi.org/10.1038/ncomms9092.
17. Sareh, S., & Rossiter, J. (2012). Kirigami artificial muscles with complex biologically inspired morphologies. *Smart Materials and Structures, 22*(1), 014004. https://doi.org/10.1088/0964-1726/22/1/014004.
18. Chen, Y., Liang, Q., Ji, C.-Y., Liu, X., Wang, R., & Li, J. (2022). A magnetic actuation scheme for nano-kirigami metasurfaces with reconfigurable circular dichroism. *Journal of Applied Physics, 131*(23), 233102. https://doi.org/10.1063/5.0091180.
19. Jang, N.-S., Kim, K.-H., Ha, S.-H., Jung, S.-H., Lee, H. M., & Kim, J.-M. (2017). Simple Approach to High-Performance Stretchable Heaters Based on Kirigami Patterning of Conductive Paper for Wearable Thermotherapy Applications. *ACS Applied Materials & Interfaces, 9*(23), 19612-19621. https://doi.org/10.1021/acsami.7b03474.
20. Frolov, Y., Bobukh, O., Samsonenko, A., & Nurnberger, F. (2023). Patterning of Surfaces for Subsequent Roll Bonding in a Low-Oxygen Environment Using Deformable Mesh Inlays. *Journal of Manufacturing Processes, 7*(5), 158. https://doi.org/10.3390/jmmp7050158.
21. Nosko, M., Konovodov, D., Samsonenko, A., & Bobukh, O. (2022). Determination of the dedormation parameters of the steel reinforcing phase inside the aluminum matrix during hot rolling. *Naukovyi Visnyk Natsionalnoho Hirnychoho Universytetu,* (6), 84-89. https://doi.org/10.33271/nvngu/2022-6/084.
22. Frolov, Y., Nosko, M., Samsonenko, A., Bobukh, O., & Remez, O. (2021). Roll Bonding of Al-Based Conposite Reinforced with C10 Steel Expanded Mesh Inlay. *Metals, 11*(7), 1044. https://doi.org/10.3390/met11071044.
23. Chen, S. H., Chan, K. C., Han, D. X., Zhao, L., & Wu, F. F. (2019). Programmable super elastic kirigami metallic glasses. *Materials and Design, 169*, 107687. https://doi.org/10.1016/j.matdes.2019.107687.
24. Isobe, M., & Okumura, K. (2016) Initial rigid response and softening transition of highly stretchable kirigami sheet materials. *Scientific Reports, 6.* https://doi.org/10.1038/srep24758.
25. Frolov, Y., Stolbchenko, M., Grydin, O., Makeeva, H., Tershakovec, M., & Schaper, M. (2019). Influence of strain parameters at rolling on the properties of wire-reinforced aluminium composites. *International Journal of Material Forming*, *12*(4), 505-518. https://doi.org/10.1007/s12289-018-1431-6.
26. *QForm UK. Windows; Micas Simulations Limited: Oxford, UK, 2023.* Retrieved from https://qform3d.com.

Трансформація деформованої кіригамі структури під час прокатки-з'єднання

Я. В. Фролов, Д. В. Коноводов, О. С. Бобух, В. В. Бояркін*

Український державний університет науки і технологій, м. Дніпро, Україна
* Автор-кореспондент e-mail: d.v.konovodov@ust.edu.ua

Мета. Кількісна оцінка деформації комірок деформівної вкладки типу кіригамі при прокатці-з'єднанні з використанням різних матриць з метою прогнозування поведінки армуючої фази в середині композиту.

Методика. Для виготовлення тришарових композитних листів використовувався процес прокатки-з'єднання. В якості армуючої фази використовувалася просічно-витяжна сітка з м'якої та нержавіючої сталі. У листах використовувалися дві матричні фази зі сплавів міді та алюмінію. Досліджені трансформації армуючої фази всередині композитного листа.

Результати. У ході дослідження отримані експериментальні дані щодо трансформації вкладки типу кіригамі, розташованої в центрі тришарових листів, під час прокатки-з'єднання. Було продемонстровано, що збільшення м'якості матриці призводить до більшого осьового плину металу в зоні деформації. Це призводить до помітного збільшення кута нахилу сітки. Наявність жорсткої матриці призводить до сплющування комірок сітки, а не до зміни їх кута. І навпаки, за відсутності матриці прокатка сталевої сітки призводить до мінімальної зміни кута сітки, поки обтиск при прокатці не досягне 50 % або більше.

Наукова новизна. У роботі вперше представлено кількісний аналіз зміни геометрії деформованої вкладки типу кіригамі в залежності від величини деформації та механічних властивостей матеріалу матриці під час прокатки-з'єднання. Розуміння зміни форми фази, що армує, у середині композитного листа полегшить прогнозування величини площі контакту матеріалу матриці при прокатці-з'єднанні.

Практична значимість. Результати, отримані в роботі, можуть бути використані для прогнозування форми кінцевої кіригамі структури в середині композитів.

Ключові слова: *прокатка-з'єднання, просічно-розтяжна сітка, алюмінієва матриця, мідна матриця*

The manuscript was submitted 07.08.24.